

Atomic-Scale Study of in Situ Metal Nanoparticle Synthesis in a Ni/TiO₂ System

Peng Li,^{*,†} Jingyue Liu,[‡] Nabin Nag,[§] and Peter A. Crozier[†]

Center for Solid State Science, Arizona State University, Tempe, Arizona 85287-1704, Monsanto Company, 800 North Lindbergh Boulevard, St. Louis, Missouri 63167, Process Technology Group, Engelhard Corporation, 23800 Mercantile Road, Beachwood, Ohio 44122

Received: December 20, 2004; In Final Form: May 3, 2005

The nucleation and evolution of Ni nanoparticles during reduction of a Ni(NO₃)₂·6H₂O precursor supported on a commercial titania substrate have been studied in situ at atomic resolution using environmental transmission electron microscopy. An incipient wetness technique was used to prepare the starting unreduced material (10 wt % Ni precursor on titania). The Ni precursor, before reduction, shows a nonuniform distribution over the titania support. It is observed that upon reduction, the initial Ni “seed” crystal nucleates within the precursor patch. The distribution and size of the Ni nanoparticles thus generated are influenced by the distribution and size of the precursor patches. In this system, we see no evidence of preferential nucleation of Ni particles on anatase or rutile. At 350 °C with CO as the reducing agent, the {111} surface facets of the Ni nanoparticles are predominant during the initial stage of nucleation and growth. However, the {111} facets are partially consumed with time, indicating that they are not thermodynamically favored in the CO atmosphere. In CO and H₂ atmospheres, Ni particles show a nonwetting morphology on titania, while in a mild oxidizing environment, a thin layer of NiO_x is formed, thus giving rise to a morphology that is indicative of wetting of the support. This work provides fundamental information on understanding and controlling the important parameters involved in the preparation of a well-designed supported Ni catalyst using the incipient wetness technique.

I. Introduction

The size, distribution, shape, and structure of supported metal nanoparticles may strongly influence the catalytic properties in ways that are difficult to understand.¹ For example, Haruta et al.² found that the finely dispersed gold particles on a select metal oxide support possess an extremely high catalytic activity, and the catalyst activity is usually attributed to the gold particles below 5 nm.³ In Ni/silica systems, Coulter et al.⁴ and Goodman⁵ have shown that the activity for hydrogenolysis of ethane is higher on Ni {100} surfaces, as compared with other surfaces. These studies demonstrate the importance of precisely controlling the size and morphology of nanoparticles in order to optimize catalytic properties. Nucleation and growth mechanisms for metallic nanoparticles or films deposited on single-crystal oxide substrates have been studied extensively,^{6–10} and they are relatively well understood. However, the typical structure of many heterogeneous catalysts consists of nanometer sized metal particles dispersed over a high-surface-area support. Moreover, in many practical applications, these materials are synthesized via incipient wetness techniques.¹¹ Very few fundamental studies have been undertaken at the atomic level to understand the underlying physical processes taking place during such synthesis. This is partly due to the complex nature of the high surface-area supports, which typically consist of particles with different sizes, crystal facets, and heterogeneous composition. However, it is possible to follow the synthesis of such complex nanoparticle systems using in situ atomic resolution environmental transmission electron microscope (ETEM).

We have employed this technique to study metal nanoparticle nucleation and evolution during the reduction of a metal precursor on a high surface-area oxide support. With such an approach, we were able to examine some of the fundamental synthesis processes.

We studied the nucleation of Ni nanoparticles on a high surface-area TiO₂ support. The Ni/TiO₂ system is suitable for such a study because it has features similar to many industrial catalysts. It consists of a catalytically active transition metal dispersed on a high-surface-area, reducible support. For many applications, a mixture of anatase and rutile is used because it gives rise to improved catalytic performance. For example, in selective oxidation reactions, Ni, supported on TiO₂ (i.e., normally a mixture of anatase and rutile phases), was found to have a greater resistance toward carbon contamination and Ni sintering,¹² as compared with other supports. Unlike other competitive systems such as Pt or Pd on Al₂O₃ or SiO₂, Ni/TiO₂ catalysts are cheaper and do not suffer as much from coking and poisoning. Therefore, the latter is an attractive industrial catalyst system. Being rather simple in composition, Ni/TiO₂ is considered as a good system for studying the genesis of the Ni nanoparticles in a supported Ni catalyst using microscopic techniques.

Advanced characterization techniques, such as scanning tunneling microscopy (STM), have been used to study dynamic nucleation and growth of Ni nanoparticles (or islands) on single-crystal rutile {110} under ultrahigh vacuum⁷ or low gas pressures (i.e., about 10⁻⁷ Torr).¹³ However, modern ETEM allows gas–solid reactions to be studied at atomic resolution in pressures up to 10 Torr.^{14–19} TEM techniques are not limited to single crystal samples and can be used to study the genesis of metal nanoparticles on high surface-area oxide supports.

* Corresponding author.

† Arizona State University.

‡ Monsanto Company.

§ Engelhard Corporation.

Therefore, the information gathered from such experiments will be of great value in designing and manufacturing industrially important catalysts.

In the present work we report on the mechanism, at the atomic scale, of the synthesis of Ni nanoparticles from a Ni nitrate hydrate precursor supported on titania under several different reducing environments (i.e., CO, H₂ and vacuum). The relationship between the size and distribution of the supported precursor and those of the Ni nanoparticles generated under different reducing environments is discussed in detail. The wetting behavior of the Ni nanoparticles formed under different reducing environments is also discussed.

II. Experimental Section

A. Precursor Preparation. Titanium dioxide (Degussa P-25, a mixture of about 75% anatase and 25% rutile) was loaded with the desired amount of Ni by an incipient wetness technique as described below. A calculated volume of an aqueous solution (just enough to fill the pores of the support), containing Ni(NO₃)₂·6H₂O, was added to a certain amount of the titania support with constant mixing. After the solution was added, the wet mass was left on an evaporating dish for 30 min in open air. The material was then dried in air at 120 °C for 16 h in a drying oven. This was the starting material that was used for further investigation. For examination by conventional TEM specimens were prepared by dispersing the precursor over holey carbon films supported on Cu grids. Samples for the in situ synthesis study of Ni nanoparticles were prepared by dispersing the precursor over 50-mesh Pt grids with 99.997% purity.

B. Synthesis of Ni Nanoparticles. In situ synthesis of the Ni nanoparticles was performed in a Tecnai F-20 field emission ETEM operating at 200kV with a point resolution of 0.20 nm.²⁰ The gas reaction cell (essentially a flow microreactor) of this instrument allowed us to perform atomic level observations of gas–solid reactions at pressures up to 8 Torr. High-resolution electron micrographs (HREM) were acquired with a Gatan video camera and stored on digital videotape during the in situ ETEM experiments. Individual frames were extracted from the videotape using the IMovie software. HREM images were also recorded with a Gatan CCD camera using the DigitalMicrograph 3.1 software. The ETEM was also equipped with a Gatan Imaging Filter permitting electron energy-loss spectroscopy (EELS) to be employed to perform high spatial resolution nanochemical analysis.²¹ Nanoanalysis was performed by placing a nanometer-sized electron probe on the nanoparticles.

Ni nanoparticles were synthesized by performing in situ reduction of the titania-supported dry precursor at 350 °C under different reducing conditions. The samples were loaded into a Gatan Inconel heating holder and 50 Torr of the reducing gases was admitted into the environmental cell for 30 min to purge the microscope before the samples were inserted into the microscope. This purging procedure reduces the concentration of background gases in the reaction cell. (It should be noted that under typical conditions in our cell, the reactive gas pressure is 7 orders of magnitude higher than the background gas pressure). The initial morphology and the nanostructure of the precursor (that is, the unreduced Ni-phase on titania) and the titania support were characterized at room temperature prior to the reduction. Reducing gas was then admitted to the reaction cell and the sample temperature ramped up to 350 °C over a period of 5 min. A rapid temperature increase was used to simulate the condition that is generally used for making metal particle catalysts. The temperature was kept constant for up to 5 h and the data were recorded every 30 min to follow the

evolution of individual Ni nanoparticles. To explore the influence of the reducing environment on the synthesis process, the Ni precursor was reduced under both strong (i.e., 0.2 Torr of 5% CO/95% N₂, 0.2 Torr of 5% H₂/95% N₂) and weak (i.e., the background vacuum of the microscope with 10⁻⁷ Torr) reducing environments.

Special experimental precautions were taken to ensure that there was not significant electron-beam induced nucleation and growth of the nanoparticles. The electron beam was blanked during most of the experiments and turned on to record data only for short periods of time in order to avoid irradiation effects. Comparison between the irradiated and nonirradiated areas demonstrated that the low electron irradiation did not cause observable effects on the in situ reduction process of the samples. This confirms that the observed changes were caused by thermal and chemical effects only. During the rapid temperature ramping, it was not possible to observe the samples with atomic resolution because of the severe thermal drift in the TEM heating holder. For this reason the first observation at 350 °C was made about 20 min after the start of the heating.

C. Characterization of the Titania Support. Additional nanoscale characterization of the morphology and structure of the titania support was carried out with a JEOL 2010F 200kV Schottky field-emission scanning transmission electron microscope (STEM). HREM and Z-contrast images²² were taken from 20 different places of the titania support. The Gatan DigitalMicrograph 3.7.1TM software was used for acquiring both HREM and Z-contrast images.

III. Results

A. Characterization of Ni Precursor on Titania Support. The titania (Degussa P-25) support is a mixture of about 75% anatase and 25% rutile. It is important to distinguish the anatase phase from the rutile phase in order to determine whether there are some special sites on the different phases of the titania grains upon which Ni particles could nucleate preferentially. Even though both the anatase and rutile phases have tetragonal crystal structures, the largest lattice spacing is 0.35 nm for anatase, corresponding to {101} atomic planes, and 0.32 nm for rutile, corresponding to {110} atomic planes. Thus, it is possible to distinguish anatase from rutile by measuring the lattice spacings from HREM images of the titania support.

Figure 1 shows a representative HREM and a Z-contrast image of the titania support. In the figure, thick areas of the sample appear with dark and bright contrast in the HREM and Z-contrast images, respectively.²² As shown in Figure 1a, the titania support is composed of separate anatase and rutile crystallites. A representative Z-contrast image of the titania (Figure 1b) shows that agglomerated titania support has a grain size of 10–50 nm.

The initial morphology, structure, and dispersion of the Ni precursor (i.e., Ni(NO₃)₂·6(H₂O)) on the titania support were studied prior to reduction and the results are shown in Figure 2. On samples with low metal loading (not shown here), most of the precursor is in the form of thin layers covering the titania surface. In this high metal loading sample, we also observe a large fraction of the precursor in the form of large patches. Many precursor patches show atomic fringes (Figures 2a–c) with lattice spacings of 0.51 and 0.47 nm corresponding to (101) and (111) atomic planes of a triclinic Ni precursor phase. Notice that the patches of the precursor are randomly distributed on the titania support. In Figures 2a,b one observes anatase (lattice spacing of 0.35 nm) as the support for the precursor, whereas in Figure 2d rutile (lattice spacing of 0.32 nm) is the support.

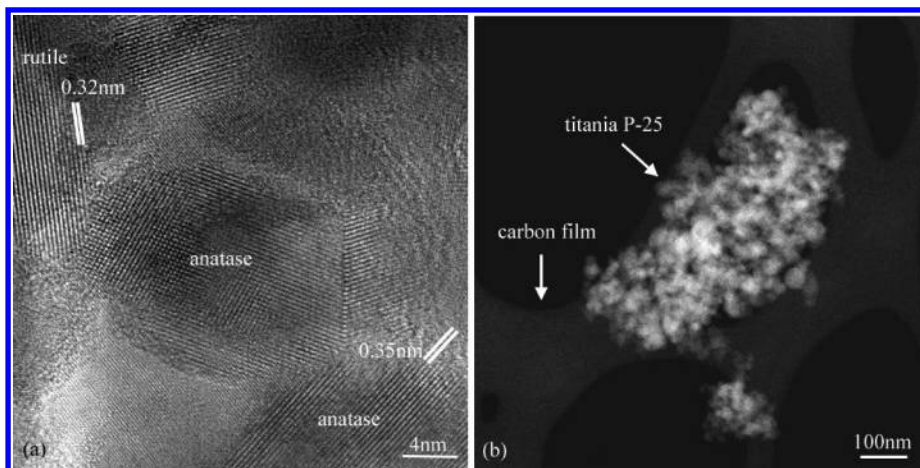


Figure 1. (a) HREM and (b) Z-contrast images of titania P-25.

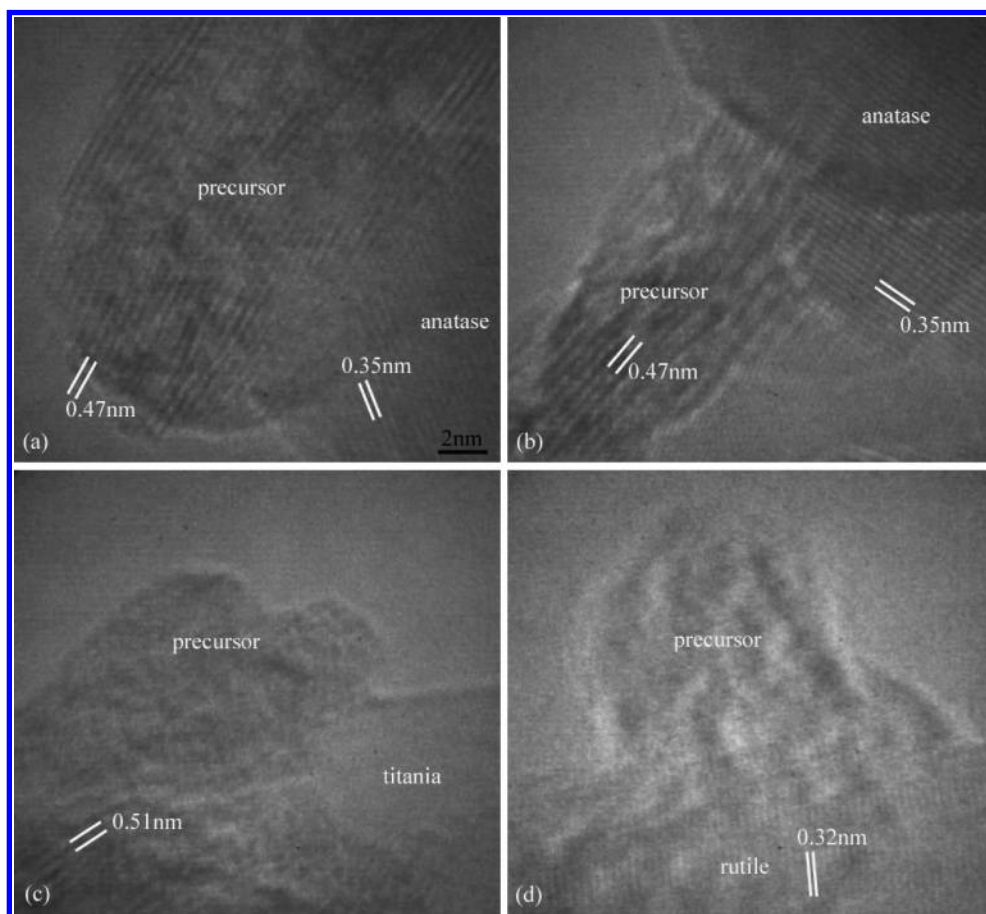


Figure 2. HREM images of the initial distribution of the Ni precursor on titania support before reduction.

These results indicate that the precursor initially gets fixed on both the anatase and the rutile phases of the titania support without showing any preference.

B. In Situ Synthesis Under Strong Reducing Conditions.

The HREM images of Figure 3 show the time evolution of the nucleation and growth of typical Ni particles as a result of the reduction of the Ni(NO₃)₂·6(H₂O) precursor in a CO atmosphere. Notice in Figure 3a (i.e., HREM image before reduction) the presence of one patch of the Ni precursor with 0.51 nm lattice spacing corresponding to (101) atomic planes on the surface of the titania support (as indicated by a white arrow). Upon reduction, this patch of the precursor directly transforms into a Ni metal nanoparticle, as shown in Figures 3b–d. The

generated Ni particle size is proportional to the size of the original precursor patch.

After 20 min of reduction (Figure 3b), the {111} Ni surface facet is dominant at this early stage of the heating and the length of other surface facets (indicated by white arrows) are comparatively short. These facets are generally the low-energy surfaces of the metal particles.²³ After 60 min at 350 °C, the Ni nanoparticle slightly increases in size but the overall shape of the particle does not change much, as seen in Figure 3c. At the final stage of the reduction (i.e., 120 min), other surface facets start to grow at the expense of the {111} surface facet. Figures 4a–c show another example of the dynamic transformation of the surface facets as a function of the time of reduction.

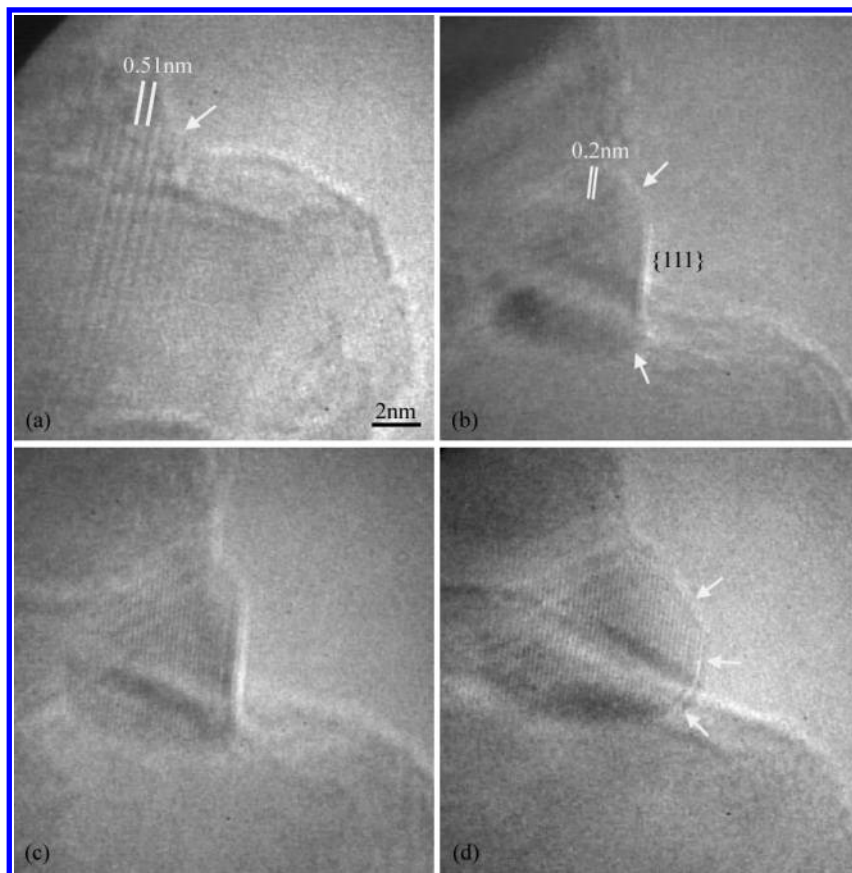


Figure 3. A series of in situ HREM images showing the nucleation and growth of Ni particles on titania support in 10 wt % Ni/TiO₂ catalysts: (a) before reduction, and (b–d) after reduced the precursor for 20, 60, and 120 min under 0.2 Torr of 5% CO/N₂ at 350 °C.

Once again, as time passes, new surface facets, marked by white arrows in Figures 4b,c, start to form and grow at the expense of the original {111} surface facets. The presence of free {111} and {100} crystal facets (free means the facet does not touch support) in a Ni nanoparticle oriented along a low-index $\langle 110 \rangle$ zone axis is clearly shown in Figure 4d. In this figure, it is observed that the {100} surface facet is 8.0 nm long and the {111} surface facet is 6.7 nm after 300 min heating. The length of the surface facets from a nanoparticle perfectly oriented along low index zone axis is directly related to the surface free energy of these surface facets,²⁴ and this issue will be discussed further in section IV.

On close inspection it is found in Figures 3d and 4c,d that most of the Ni nanoparticles have a nonwetting morphology after 300 min reduction. The Ni nanoparticles are considered to have a nonwetting morphology when the contact angles (i.e., the angles between tangent line of the surface of Ni particle and the Ni/titania interface) are larger than 90°. Notice that there is a transformation from wetting to nonwetting morphology with time in Figures 4a–c. Figure 4d also shows that there is no atomic plane matching of the Ni nanoparticle and anatase support across the Ni/TiO₂ interface in the figure.

Similar results on the morphology of the Ni nanoparticles are obtained when the reduction is performed in a hydrogen atmosphere. Figure 5 shows typical HREM images of the Ni nanoparticles that are generated after the precursor is reduced in situ for 180 min. These images confirm that the morphology of the reduced Ni nanoparticles is nonwetting.

To clarify the relationship between the size and distribution of the precursor and the Ni nanoparticles, HREM images of two Ni nanoparticles, after having the precursor reduced in situ

for 180 min under 5% H₂/N₂, are given in Figure 6. Notice that the dramatic size difference between the two particles (i.e., 14 nm in Figure 6b versus 5 nm in Figure 6d) is correlated with the difference in the initial size of the precursor patches shown in Figures 6a,c. Also notice that the Ni particles stay at the same location as the Ni precursors before the reduction. These results indicate that in this high metal loading case, the size and distribution of the Ni nanoparticles formed after reduction correlate with the initial size and distribution of the precursor patches.

C. In Situ Synthesis Under Weak Reducing Conditions.

HREM images taken during in situ synthesis of Ni nanoparticles performed under weak reducing conditions (i.e., ambient vacuum of microscope) are shown in Figure 7. In Figure 7a, the patch of material, indicated by an arrow, is the Ni(NO₃)₂·6(H₂O) precursor. After 60 min of heating in a vacuum, this patch of the precursor partially transforms into a Ni particle as evidenced by the presence of Ni metal {111} fringes (see Figure 7b). Notice that the remaining precursor-like contrast at the surface of the Ni particle (indicated by a white arrow in Figure 7b) disappears after longer heating time (Figures 7c,d). The sizes of the precursor patch in Figure 7a and of the reduced Ni particle in Figure 7d are about the same (i.e., 10 nm). Moreover, most Ni nanoparticles still have a wetting or half-cup morphology after heating for 300 min, as shown in Figures 7d,e. The Ni particles are coated by an overlayer (indicated by an arrow in Figure 7e). To identify this overlayer, EELS spectra were acquired from the surface of the Ni particles using a 0.5 nm electron probe and the result is shown in Figure 7f. This nanospectroscopic result shows two edges corresponding to the

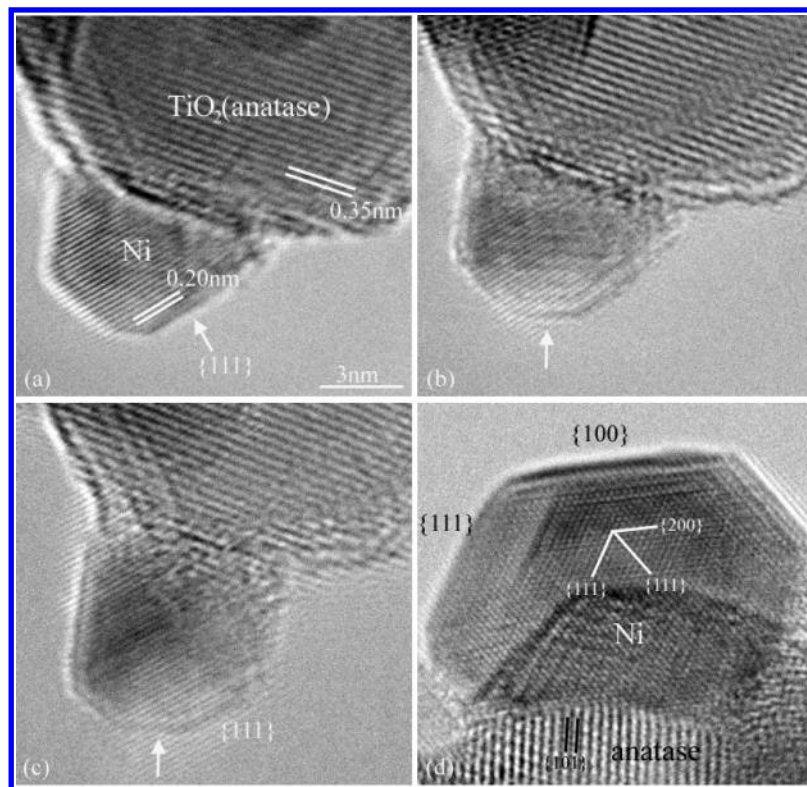


Figure 4. In situ HREM images showing the shape changing of the Ni particles on titania support in 10 wt % Ni/TiO₂ catalysts as the Ni precursor was reduced in 0.2 Torr of 5% CO/N₂ at 350 °C for (a) 90, (b) 102, and (c) 180 min. Most Ni particles have nonwetting morphology as shown in panel d after reduced for 300 min.

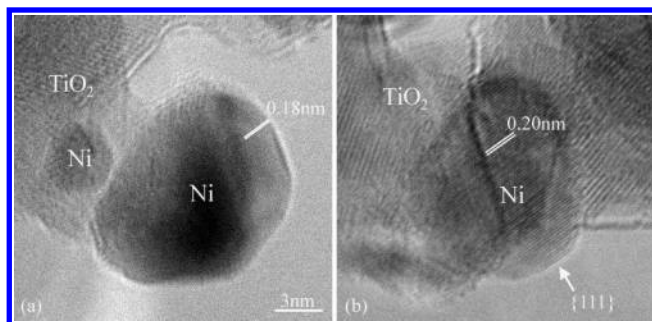


Figure 5. In situ HREM images showing the nonwetting morphology of most Ni particles on titania support as the Ni precursor was reduced in 0.2 Torr of 5% H₂/N₂ at 350 °C for 180 min.

oxygen K-edge (at 532 eV) and Ni L_{2,3}-edges (at 855 eV), indicating that this surface overlayer is NiO_x.

IV. Discussion

A. Initial Nucleation and Growth of Ni Nanoparticles. In this high metal loading samples, the nucleation sites of the Ni nanoparticles depend primarily on the locations of the precursor patches before reduction, as presented in section III. Ni nanoparticles are found to nucleate on both anatase and rutile supports due to the random distribution of Ni precursor on the titania support. These results are different from those on Au/TiO₂²⁵ and Pt/TiO₂²⁶ systems, where Au and Pt nanoclusters nucleate preferentially on the rutile support. This difference may be caused by differences in the interactions between the precursors and the two forms of titania. For example, there might exist a preferential chemical bond between Au(OH)₃ (i.e., the precursor used in Au/TiO₂ system²⁵) and rutile grains, which results in the preferential nucleation of Au cluster on the rutile grains. This indicates that a careful selection of the precursor can probably lead to finer control over the nucleation sites of

the Ni nanoparticles on the support in the Ni/TiO₂ catalyst system.

The initial conversion of the Ni nitrate hydrate patches to the Ni nanoparticles under CO is relatively fast (i.e. nearly completed during the first 20 min of reduction). The particle continues to grow at a slower rate as reduction continues and after 120 min no further growth is observed indicating that the precursor is completely transformed to Ni. In addition, the Ni particles do not move during the heating at 350 °C, indicating that particle coalescence is not responsible for the growth of the Ni particles at this temperature. This is consistent with other works reporting that significant coalescence of the metallic nanoparticles does not take place until the reduction temperature reaches 500 °C.

The nucleation and growth rate of Ni nanoparticles from the precursor under weaker reducing environments (i.e., vacuum) is much slower than that under CO or H₂. Some portion of the precursor remains unreduced at the surface of the Ni particle even after 60 min of reduction. This demonstrates that modification of the reducing environments can be used to control the nucleation and growth rates of the Ni nanoparticles on titania. The slower synthesis rate associated with the weaker reduction environment also allows the Ni nucleation process to be recorded at an earlier stage of the reduction process. The HREM images of Figure 7 show that the growing Ni particle is surrounded by a partially reduced shell of the precursor, indicating that the Ni metal nucleation does not take place at the surface of the precursor particle. The data suggest that the initial metal nucleation occurs in the large precursor patch either at the interface with the titania support and/or in the center of the precursor patch. This initial nanocrystallite acts as the seed crystal for subsequent metal particle growth.

It is interesting that for all reduction environments used in this study, the size of the final Ni particle and the precursor

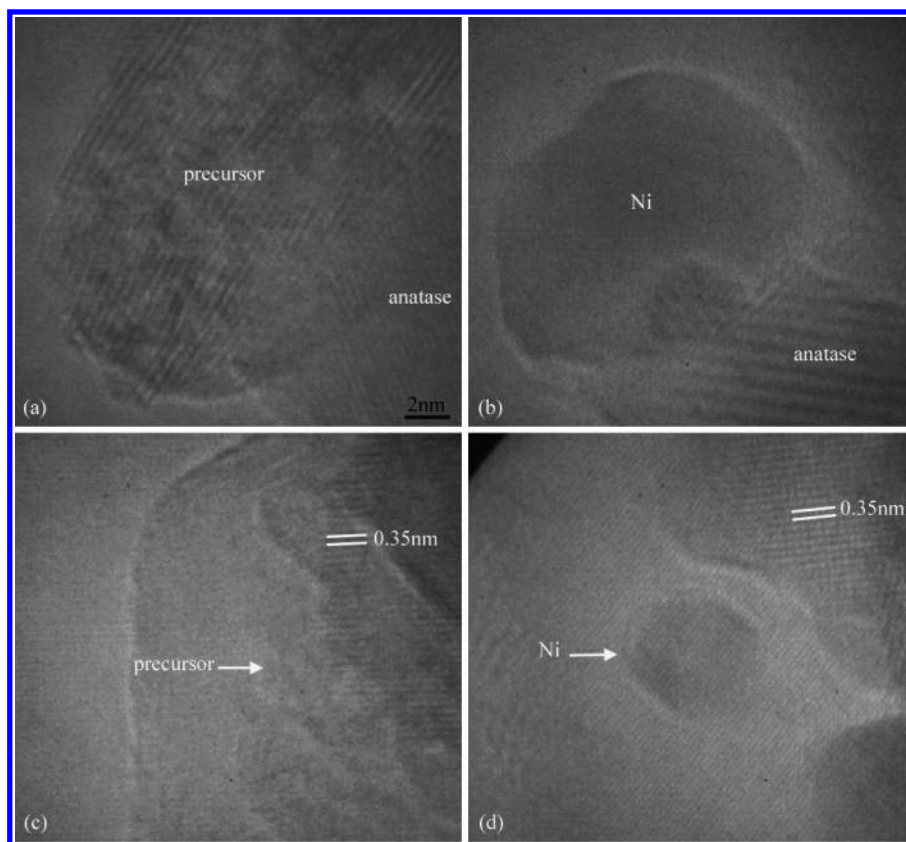


Figure 6. (a, c) HREM images of the precursor before reduction and (b, d) the Ni particles after 180 min reduction under 5% H_2/N_2 .

patch agree to within a factor of 2. However, when a $\text{Ni}(\text{NO}_3)_2 \cdot 6\text{H}_2\text{O}$ patch transforms to face-centered-cubic (fcc) Ni metal, the final particle size should drop by approximately a factor of 3. The volume decrease occurs because of the extensive mass loss that occurs during the reduction and because of the denser packing of Ni atoms in the fcc metal particle. Since we usually observe Ni particles sizes within a factor of 2 of the precursor patches this shows that many of the Ni atoms in the final nanoparticles were not present in the original precursor patch. Our measurements suggest that more than 80% of the Ni atoms have diffused into the growing metal seed crystallite from adjacent precursor layers on the surface of the titania. The correlation between the Ni particle size and the precursor patch implies that large patches are associated with large local surface coverages and small patches are associated with small local surface coverages. This shows that the precursor coating the titania surface is not uniform and is associated with the presence of patches.

Our results demonstrate the importance of carefully controlling the distribution of precursor on support. For high metal loadings, metal particle size depends on the location of precursor patches since these are the nucleation centers in this case. Important parameters for precursor preparation will include the way the precursor is loaded and fixed on the support (that is, dry or wet impregnation; the pH of the salt solution used for impregnation, aging, drying etc.). By carefully studying and optimizing these parameters, a uniform size and distribution of the initial precursor on the support may be achieved, which in turn may yield the desired size and distribution of metal nanoparticles.

B. Evolution of Ni Nanoparticle Surface Facets Under CO Environment. The modification of the surface facets to achieve a certain desired structure of the nanoparticles is very important in the area of heterogeneous catalysis. For example, it has been

shown that the activity for hydrogenolysis of ethane on Ni {100} is higher than that on Ni {111}.⁵ This is due to the fact that the distance between two hollow sites on Ni {100} is much larger than the C–C bond (0.15 nm); thus, the dissociation of the ethane molecule is favored on the Ni {100} face than on the Ni {111} wherein the distance between two hollow sites is 0.14 nm.⁵ One practical approach for modifying the relative distribution of surface facets is to change the reducing gases. This may cause a change in the free energies of different surfaces because of differential adsorption of gas molecules on the surfaces of the metallic particles. Hansen et al.¹⁷ have shown that the {111} surface facets of Cu transform to {110} and {100} facets in a Cu/ZnO model catalyst as the reducing gas was changed from pure H_2 to a mixture of H_2 and water.

In situ ETEM allows us to follow the evolution of the surface structure of individual nanoparticles.¹⁵ During reduction in a CO environment, Ni {111} surfaces are formed within the first hour of the nucleation and growth processes. As time passes, other low-energy surface facets (i.e., most likely {100} and {110}) develop at the expense of the {111} facets. The size and shape of the nanoparticles do not change significantly after 120 min of heating implying the attainment of the equilibrium of particle shape in 120 min.

In general, the {111} surface of fcc metal nanoparticles has a lower energy than those of {110} and {100} surfaces under ultrahigh vacuum conditions.²⁸ However, the anisotropy of surface free energy can be inverted by the adsorption of gases on the metal surface.²³ For example, the adsorption energy of CO, calculated by a tight binding approach, increases in the order of {111}, {100} and {110} surfaces in Pd with similar fcc crystal structures.^{29,30} Thus, it is possible that CO might be adsorbed more strongly on the Ni {100} and {110} surfaces compared to the Ni {111} surface, resulting in lower free energies of Ni {100} and {110} surfaces compared to that of

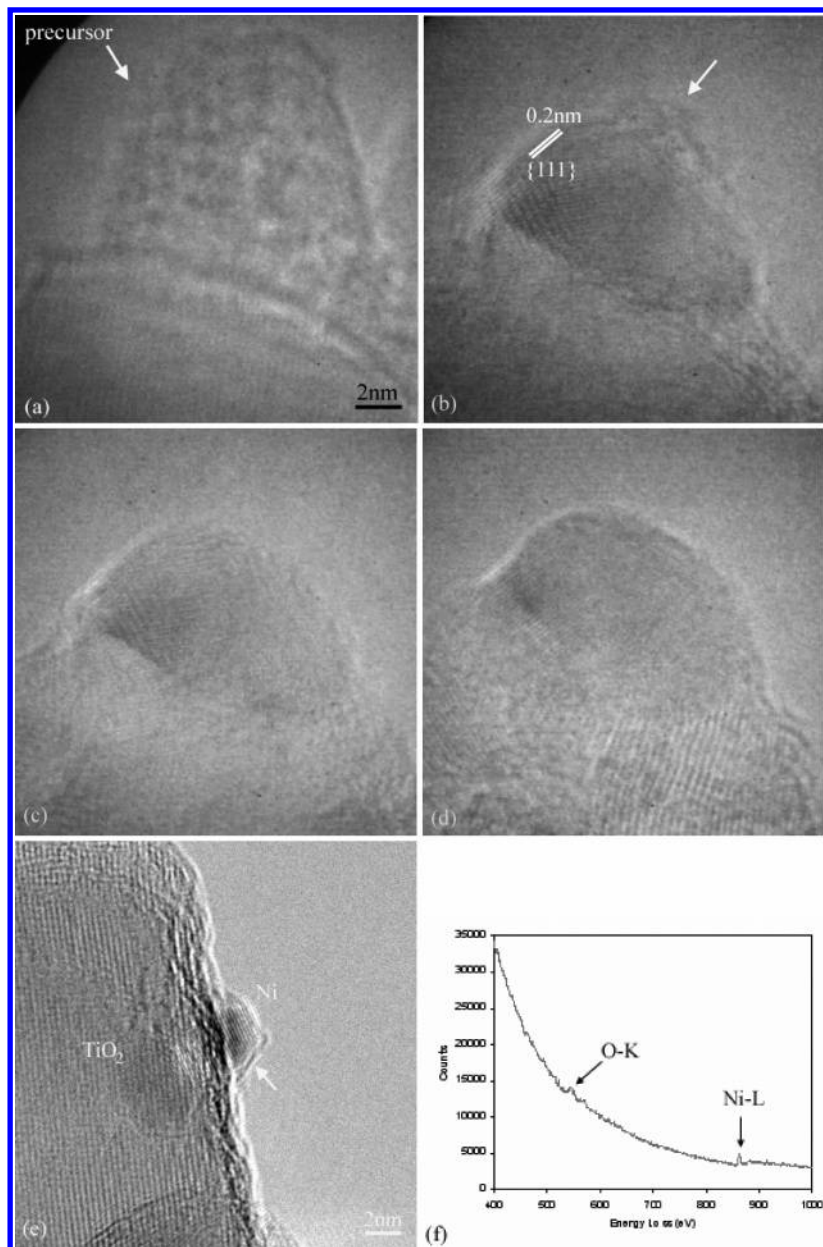


Figure 7. A series of in situ HREM images showing the synthesis of 10 wt % Ni/TiO₂ catalysts at 350 °C: (a) before reduction, (b–d) after reduced the precursor for 60, 120, and 300 min, (e) the representative shape of the particles after reduced for 360 min, and (f) the corresponding EELS spectrum from the surface of the Ni particle.

Ni {111} in a CO atmosphere. We know from the experiment carried out in a vacuum that the initial Ni nucleation occurs inside the nitrate precursor. Consequently the initial surface faceting will be strongly influenced by the presence of unreduced precursor on the metal surface. This may explain why we initially see a strong {111} facet which is gradually consumed by new lower energy surfaces when exposed directly to the CO environment.

Comparison of the relative lengths of different facets in the equilibrium shape of the nanocrystals provides strong experimental evidence for the above hypothesis. In the equilibrium crystal shown in Figure 4d, the length of the {100} surface facet is 8.0 nm while that of the {111} facet is only 6.7 nm. This indicates that the surface free energy of Ni {100} is 16% lower than that of {111} under CO at 350 °C, since the longer surface facet has lower surface energy.²⁸ Similar phenomenon due to the stronger absorption of O₂ on the {100} surface than on {111} surface of Pd nanoparticles has also been observed in a Pd/MgO model catalyst, where the {100} facets of Pd develop at

the expense of the {111} facets before the formation of PdO under O₂ environment.³¹ The modification of the surface Pd facets involves self-diffusion of atoms from {111} to other low-energy surfaces. In our measurements, the other facets grow at the expense of the {111} facet (see Figures 3 and 4) showing that, in the Ni system, the surface modification also involves self-diffusion from the {111} surface.

C. Reduction Environments Versus the Wetting Behavior of Nanoparticles. The wetting behavior of the metallic nanoparticles on the oxide support is mainly described by the following equation:²⁷

$$\gamma_o = \gamma_{m/o} + \gamma_m \cos\theta$$

where θ is the contact angle between the metallic particle and the oxide support, γ_o and γ_m are the surface energies of the oxide and the metal, respectively, and $\gamma_{m/o}$ is the interfacial energy between the metallic particle and the oxide. From this equation the contact angle θ is larger than 90° giving the nonwetting behavior showing that γ_o must be smaller than $\gamma_{m/o}$.

As in our Ni/TiO₂ system, most Ni nanoparticles do not wet the titania support and have well-faceted shape under the CO and H₂ reduction environments. More importantly, there is no atomic plane matching of the Ni and titania across the interface (as shown in Figure 4(d) and discussed in section III), indicating that the Ni/TiO₂ interface is most likely to be incoherent.^{28,32} In general, the interfacial energy of an incoherent interface ranges from 0.8 to 2.5 J/m².²⁸ It is also known that the surface energy of titania is about 0.7 J/m² under vacuum.³³ We expect the surface energy of titania to be lower in the reducing gases because of adsorption of gas molecules onto the surface.²³ Consideration of these energies and our observations demonstrate that the nonwetting behavior of the Ni nanoparticles on a titania support is thermodynamically favored. It is also well-known that there is a strong metal support interaction (SMSI) between group VIII metals (such as Ni) and titania [27], therefore, SMSI might affect the wetting behavior of the titania supported Ni particles. However, the SMSI is normally significant at temperatures higher than 500 °C [27], and we suggest it has little effect on the wetting behavior of the Ni nanoparticles reduced at the temperature of 350 °C.

In contrast to nonwetting behavior in strong reducing conditions, the Ni nanoparticles wet the titania support under the weaker reducing environment (i.e., vacuum). In this case we observe a very thin NiO_x layer with a thickness of about 0.3–0.4 nm (i.e., one or two monolayers) coating the surface of Ni particles. The origin of the oxygen might come from the decomposition of the Ni nitrate hydrate precursor (i.e., Ni(NO₃)₂·6(H₂O)) and/or the background gases in the vacuum system. Moreover, oxygen easily bonds to the Ni surface because of a strong Ni-oxygen bonding energy (i.e., 392 kJ/mol).³⁴ The NiO_x-coated overlayer generates a NiO_x/TiO₂ interface. In general, the oxide–oxide interface has a stronger bond and thus, a lower interfacial energy than the metal–oxide interface.²⁷ This thin oxide layer causes the nanoparticles to wet the titania support. The surface oxidation of Ni is inhibited when synthesis is conducted under strongly reducing environments such as H₂ and CO.

Treatment in O₂ is recognized as an important means for redispersion of metallic nanoparticles and is applied in the industry to rejuvenate spent metallic catalysts.²⁷ A recent study on the O₂ influence on the growth mode of Cu and Ni islands on titania demonstrates that the 3-D growth of the Cu and Ni islands can transform to 2-D growth.¹³ This causes a redispersion of the Cu and Ni islands on the TiO₂ support by O₂ treatment. In our study, we find that in a slightly oxidizing environment, the thin oxide layer formed on the Ni surface causes the nanoparticle to adopt a wetting morphology. Even though only the Ni particle surface is oxidized our results demonstrate the onset of the complex redispersion phenomenon, which involves oxidizing of the metal particles and wetting and spreading of the metal oxides under strong oxidizing environment.²⁷

V. Conclusions

We have performed in situ atomic-resolution studies on Ni nanoparticle nucleation and evolution during the reduction of a metal precursor on a high surface-area titania support. Under high metal loading conditions, the unreduced precursor, prepared by an incipient wetness technique, shows a nonuniform distribution over the titania support. Upon reduction, the initial seed crystals formed in the precursor patches, and the distribution and size of the synthesized Ni nanoparticles are influenced by the distribution and size of the precursor patches. In this system,

we see no evidence for preferential nucleation of Ni particles on anatase or rutile. At 350 °C in CO, the {111} surface facets of the Ni nanoparticles are predominant during initial nucleation and growth. However, the {111} facet is not thermodynamically favored in the CO atmosphere and is partially consumed with time. In CO and H₂, metal particles show a nonwetting morphology on titania, while in a more oxidizing environment, a thin layer of NiO_x forms to give rise to a wetting morphology. This in situ ETEM work provides fundamental information for understanding and controlling important parameters for synthesizing metal nanoparticle catalyst systems using the incipient wetness route.

Acknowledgment. This research was conducted using the facilities in the Center for Solid State Science at Arizona State University and was supported by Monsanto Company. The authors thank Mr. K. Weiss for the maintenance of the Tecnai F-20 ETEM. The authors also thank Dr. R. Sharma and Dr. R.-J. Liu for the valuable discussions regarding the ETEM.

References and Notes

- (1) Haruta, M. *Catal. Today* **1997**, *36*, 153.
- (2) Haruta, M.; Tsubota, S.; Kobayashi, T.; Kageyama, H.; Genet, M.; Delmon, B. *J. Catal.* **1993**, *144*, 175.
- (3) Wolf, A.; Schüth, F. *Appl. Catal. A* **2002**, *226*, 1.
- (4) Coulter, K.; Xu, X.; Goodman, D. W. *J. Phys. Chem.* **1994**, *98*, 1245.
- (5) Goodman, D. W. *Surf. Sci.* **1982**, *123*, L679.
- (6) Zhou, J.; Kang, Y. C.; Chen, D. A. *J. Phys. Chem. B* **2003**, *107*, 6664.
- (7) Tanner, R. E.; Goldfarb, I.; Castell, M. R.; Briggs, G. A. D. *Surf. Sci.* **2001**, *486*, 167.
- (8) Diebold, U.; Pan, J.; Madey, T. E. *Surf. Sci.* **1995**, *331–333*, 845.
- (9) Wu, M.; Möller, P. J. *Surf. Sci.* **1992**, *279*, 23.
- (10) Bourgeois, S.; Jomard, F.; Perdureau, M. *Surf. Sci.* **1991**, *249*, 194.
- (11) Jos van Dillen, A.; Terörde, R. J. A. M.; Lensveld, D. J.; Geus, J. W.; De Jong, K. P. *J. Catal.* **2003**, *216*, 257.
- (12) Vannice, M. A.; Garten, R. L. *J. Catal.* **1979**, *56*, 236.
- (13) Zhou, J.; Kang, Y. C.; Chen, D. A. *Surf. Sci.* **2003**, *537*, L429.
- (14) Boyes, E. D.; Gai, P. L. *Ultramicroscopy* **1997**, *67*, 219.
- (15) Gai, P. L. *Adv. Mater.* **1998**, *10*, 1259.
- (16) Gai, P. L. *Top. Catal.* **1999**, *8*, 97.
- (17) Hansen, P. L.; Wagner, J. B.; Helveg, S.; Rostrup-Nielsen, J. R.; Clausen, B. S.; Topsøe, H. *Science* **2002**, *295*, 2053.
- (18) Wagner, J. B.; Hansen, P. L.; Molenbroek, A. M.; Topsøe, H.; Clausen, B. S.; Helveg, S. *J. Phys. Chem. B* **2003**, *107*, 7753.
- (19) Sharma, R. *Microsc. Microanal.* **2001**, *7*, 494.
- (20) Sharma, R.; Crozier, P. A.; Marx, R.; Weiss, K. *Proc. Microsc. Microanal.* **2003**, *9* (Supplement 02), 912.
- (21) Egerton, R. F. *Electron Energy-Loss Spectroscopy in the Electron Microscope*; Plenum Press: New York, 1986; pp 255–62.
- (22) Kirkland, E. J. *Advanced Computing in Electron Microscopy*; Plenum Press: New York, 1998.
- (23) Henry, C. R. *Surf. Sci. Reports* **1998**, *31*, 231.
- (24) Howe, J. M.; Mebed, A. M.; Chatterjee, K.; Li, P.; Murayama, M.; Johnson, W. C. *Acta Mater.* **2003**, *51*, 1359.
- (25) Akita, T.; Lu, P.; Ichikawa, S.; Tanaka, K.; Haruta, M. *Surf. Interface Anal.* **2001**, *31*, 73.
- (26) Iddir, H.; Disko, M. M.; Browning, N. D.; Ogut, S. *Proc. Microsc. Microanal.* **2004**, *10* (Supplement 02), 448.
- (27) Raupp, G. B.; Stevenson, S. A.; Dumesic, J. A.; Tauster, S. J.; Baker, R. T. K. In *Metal-Support Interactions in Catalysis, Sintering, and Redispersion*; Stevenson S. A., Dumesic, J. A., Baker, R. T. K., Ruckenstein, E., Eds.; Van Nostrand Reinhold Company Inc.: New York, 1987.
- (28) Howe, J. M. *Interfaces in Materials: Atomic Structure, Kinetics and Thermodynamics of Solid: Solid, Solid: Liquid and Solid: Vapor Interfaces*; John Wiley and Sons: New York, 1997.
- (29) Mottet, C.; Trégliat, G.; Legrand, B. *Surf. Sci.* **1996**, *352–354*, 675.
- (30) Sawaya, S.; Goniakowski, J.; Mottet, C.; Saul, A.; Trégliat, G. *Phys. Rev. B* **1997**, *56*, 12161.
- (31) Giorgio, S.; Henry, C. R.; Chapon, C.; Roucau, C. *J. Catal.* **1994**, *148*, 534.
- (32) Li, P.; Howe, J. M.; Reynolds, W. T., Jr. *Acta Mater.* **2004**, *52*, 239.
- (33) Bates, S. P.; Kresse, G.; Gillan, M. J. *Surf. Sci.* **1997**, *385*, 386.
- (34) Lide, D. R., Ed. In *CRC Handbook of Chemistry and Physics*; VRC Press: New York, 1997.